Al_2O_3 and Sn/Al_2O_3 nanowires: fabrication and characterisation

Mohamed Shaban[1], Mona Ali[1], Kamal Abdel-Hady[2], Hany Hamdy[1]

[1]*Department of Physics, Faculty of Science, Nanophotonics and Applications Lab, Beni-Suef University, Beni-Suef 62514, Egypt*
[2]*Department of Physics, Faculty of Science, Elminia University, Elminia, Egypt*
E-mail: mssfadel@aucegypt.edu

Published in Micro & Nano Letters; Received on 18th February 2015; Accepted on 1st April 2015

Self-ordered anodised aluminium oxide membranes can be used as a base for the growth of different nanoarrays. In this reported work, an efficient and effective method is implemented to fabricate highly ordered alumina nanowires (ANWs) covered with a uniform shell of 12 ± 2 nm Sn nanoparticles (Sn/ANWs). A two-step anodisation process followed by a selective etching process was used to prepare highly ordered ANWs with diameters smaller than 36 nm. The thermal evaporation technique was used to ensure the deposition of a Sn nanoshell on the fabricated nanowires. The fabricated nanostructures were characterised by energy-dispersive X-ray spectroscopy, X-ray diffraction, field emission-scanning electron microscopy and an ultraviolet–visible–near-infrared spectrophotometer. Analysis of the scanning electron microscopy images showed that the etching rate is 0.73 nm/min and ANWs are obtained after etching the membrane for 110 min. The measured reflection spectra revealed that Sn/ANWs exhibit a redshift of the UV absorption band relative to the ANWs and a reflectance of nearly 100% in the near-infrared region. For optical comparison, glass slides were coated with Sn under the same conditions for 90 and 120 s. The reflection spectrum of the 120 s Sn-coated glass slide shows three modes at 210, 296 and 700 nm because of the excitation and interference of plasmonic waves.

1. Introduction: In recent years, the fabrication of metal/metal–oxide nanowires has attracted much interest owing to their potential use in many applications. These structures are candidates for the development of new types of sensors, lithium storage materials, solar cells and blue and ultraviolet (UV) light-emitting diodes [1–5]. Many metals and metal oxides have been intensively studied [1–6]. In particular, tin (Sn) and tin oxide (SnO) nanostructures are usually regarded as promising future materials because of their high specific capacities, low cost and natural abundance. The specific capacities of Sn, SnO and SnO_2 are ca. 994, 875 and 782 mAh g^{-1}, respectively, which are much higher than that of the conventional graphite anode (ca. 370 mAh g^{-1}) [2–4]. In addition, Sn metal is stable at and above room temperature, malleable and weldable with copper (Cu) and aluminium (Al). Moreover, it has low electrical resistivity, a low-melting point (231°C) and high-surface tension (0.544 N/m). The fabrication and applications of Sn and SnO nanostructures have been hardly investigated compared with the facilely obtained nanowires of different metals and metal oxides [3–5]. The fabrication of Sn and SnO nanostructures still present a challenging task to experimentalists, especially nanowires and nanorod morphologies, by highly controlled and low-cost methods.

Anodised aluminium oxide (AAO) membranes with a nanoporous structure have been widely used as membranes in the fabrication of various nanostructures because of the cheap equipment, simple technology, high-throughput and high controllability of the process [7–9]. The diameter, length and shape of the fabricated nanostructures are controlled by the structural parameters of the membrane, such as the nanopores' diameter, thickness and surface morphology. Up to now, various kinds of nanowires, nanotubes, nanorods and nanoparticles have been successfully synthesised using AAO membranes [10–13]. Many different techniques have been used for the deposition of nanowires inside AAO membranes [14–16]. However, there is a strong demand for an inexpensive and reliable method that can be used to pattern nanowires in one and two dimensions. One of the most hopeful options is the use of the AAO membrane and thermal evaporation technique to obtain nanowire arrays. The thermal evaporation technique has merits such as low cost of processing, facile technology and a relatively simple equipment requirement.

In the work reported in this Letter, synthesised alumina (Al_2O_3) nanowires (ANWs) were decorated with Sn shell nanoparticles. The ANWs were fabricated by chemical etching of the AAO membrane in a phosphoric acid solution at room temperature. The Sn nanoparticles were deposited on the ANWs by the thermal evaporation technique. The structures and morphologies of the ANWs and Sn/

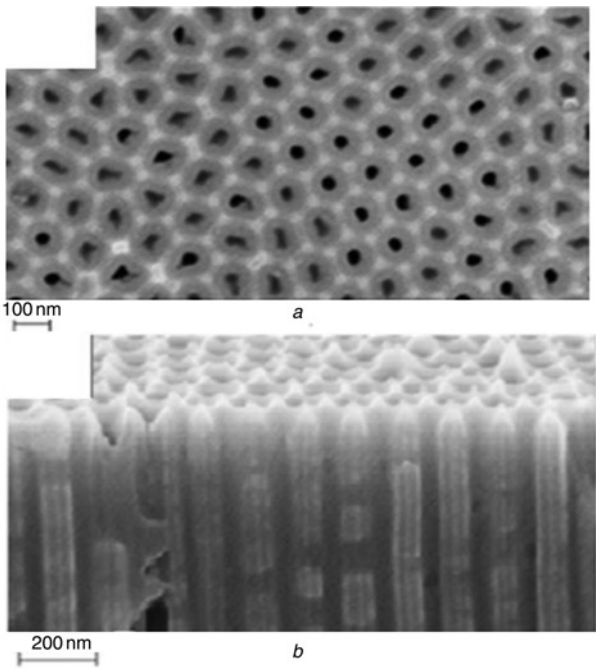

Figure 1 *SEM images of AAO membrane anodised at 50 V in 0.3 M oxalic acid for 10 min*
a Top view
b Cross-sectional view

doi: 10.1049/mnl.2015.0068

ANWs were characterised by several means including field emission-scanning electron microscopy (FE-SEM), energy-dispersive X-ray spectroscopy (EDX), X-ray diffraction (XRD) and and ultraviolet–visible–near-infrared (UV–vis–NIR) spectrophotometer.

2. Materials and methods: For the fabrication of ANWs coated with Sn shell nanoparticles, the preparation of a well built-in uniform AAO membrane is a must. High purity (99.999%) Al foils of 0.25 mm thickness were used as a starting material. The Al foils were degreased using a successive immersing process in acetone and methanol for 5 min at 150°C, and then rinsed in deionised water for 10 min. The foils were electropolished to a mirror finish in an electrochemical solution with a volume mixture of 1:1:1 H_3PO_4:H_2SO_4:H_2O at 50°C under constant stirring for 3 min. The AAO membrane was prepared by a two-step anodisation process [17]. In the first anodisation step, the clean Al foil was anodised in a 0.3 M $C_2H_2O_4$ solution at a voltage of 50 V and temperature of 9°C for 3 h. After the first anodisation, the Al_2O_3 membrane was immersed in an etching solution of H_2O, H_3PO_4 and CrO_3 (100 ml:10 ml:1 gm) for 3 h at room temperature to remove the Al_2O_3 layer. The treated Al foil was subjected to a second anodisation process under the same previous conditions for 10 min. Pore widening for the fabricated AAO membrane was carried out at 6 wt% H_3PO_4 for different lengths of time to obtain ANW arrays. By using the thermal evaporation technique (Evaporation plant, Edward, mode 6E), Sn nanoparticles were deposited on the ANWs at room temperature and at a pressure of 10^{-5} Torr for 120 s.

3. Samples characterisation: The crystal structures of the ANWs and Sn/ANWs were investigated using a high-resolution X-ray diffractometer (model: PANalytical X'Pert Pro, Holland) with CuKα radiation ($\lambda = 1.5406$ Å), operated at 45 kV and 40 mA. The XRD patterns were recorded in the 2θ range 10°–90°. The patterns were analysed by matching the observed peaks with the standard patterns provided by JCPDS files. Morphological and chemical composition studies of the fabricated nanostructures were carried out using FE-SEM (model: ZEISS SUPRA 55 VP and ZEISS LEO, Gemini Column) equipped with EDX. The optical characterisation was carried out at room temperature using a UV–vis–NIR spectrophotometer (model: LAMBDA 950, Perkin Elmer, USA) in the wavelength range 200–2000 nm.

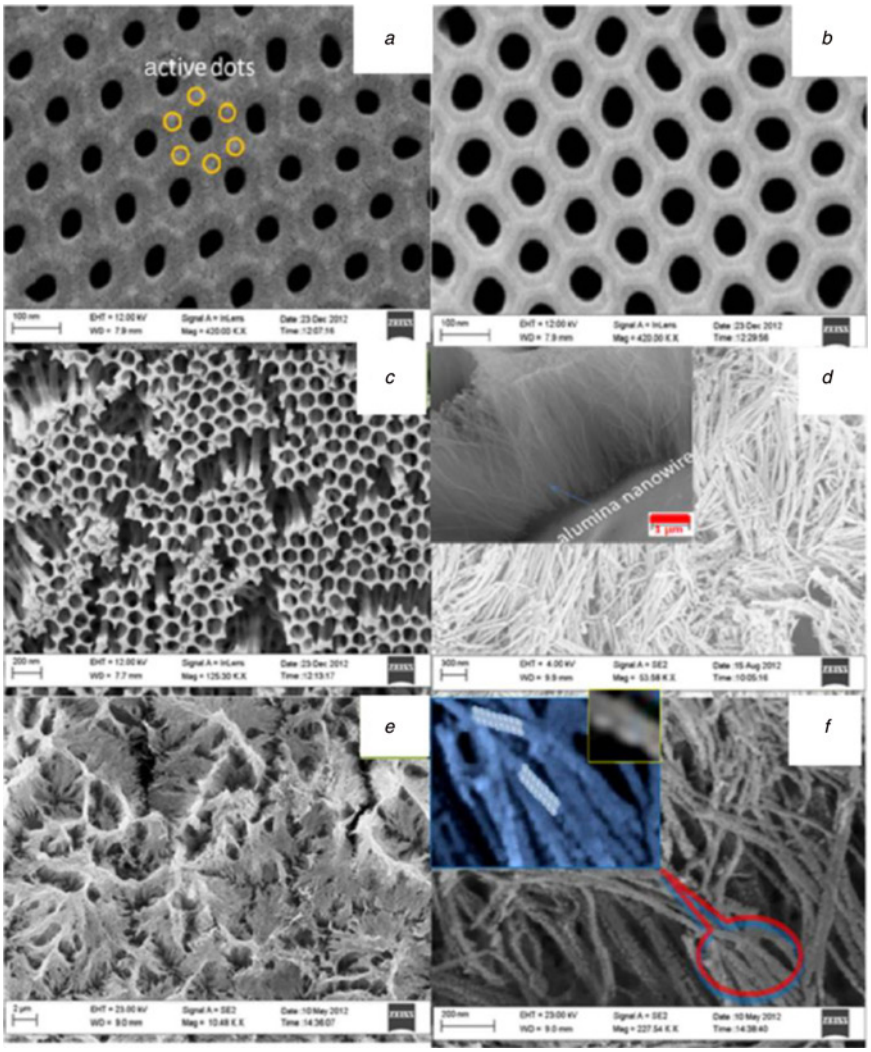

Figure 2 *SEM images of AAO and Sn/ANWs*
a AAO after etching in phosphoric acid solution for 30 min
b AAO after etching in phosphoric acid solution for 90 min
c AAO after etching in phosphoric acid solution for 100 min
d AAO after etching in phosphoric acid solution for 110 min
e Sn/ANWs at low magnification
f Sn/ANWs at high magnification

4. Results and discussion: Fig. 1 shows top view and cross-sectional view SEM images of the fabricated AAO membrane. This membrane has highly ordered and vertically aligned hexagonal nanopores perpendicular to the Al substrate. The average pore diameter is around 45 nm and the interpore distance is around 125 nm. The pore density and porosity of the AAO are 7.4×10^9 cm^{-2} and 15%, respectively.

To obtain highly ordered ANWs, a controlled etching methodology of the AAO pore walls is required to leave only an array of the pure ANWs at the corners of the hexagonal cells. Figs. 2*a*–*d* show top view SEM images of the AAO membranes at different etching times of 30, 90, 100 and 110 min, respectively. The pore diameter of the as-prepared AAO membrane is 45 nm, and the wall thickness is about 80 nm.

Table 1 shows the resulting structural parameters and morphologies for self-organised AAO membranes fabricated under the same conditions at different etching times. The data presented in this Table shows an increase in the hexagonal ordering and the uniformity of the fabricated AAO with the etching time as shown in Figs. 2*a* and *b*. The experimental data give an average etching rate of 0.73 nm/min. At 100 min etching time, as shown in Fig. 2*c*, cracks have appeared on the AAO wall, which was an indication of the formation of ANWs. Uniform sized and high-yield ANWs of the order of 2×10^{10} wire/cm^3 were produced at an etching time greater than 100 min. Fig. 2*d* shows the top view SEM image for ANWs of 1.23 µm length and 36 nm diameter. The inset of Fig. 2*d* shows a cross-sectional image of vertically aligned ANWs of length 3 µm produced by etching the fabricated AAO membrane for 110 min. Figs. 2*e* and *f* show SEM images for ANWs covered with a shell of Sn nanoparticles to form Sn/ANWs. The diameter of the Sn/ANWs is about 57 nm and the length is 1.23 µm. As shown, the Sn/ANWs inclined and aggregated into disordered domains because of the gravity field [18]. The enlarged SEM image for the fabricated Sn/ANWs, Fig. 2*f*, gave an estimated tin–shell size of 12 ± 2 nm.

The manufactured ANWs and Sn/ANWs were examined by EDX to identify possible impurities in the formation of the ANWs and to determine the percentage weight deposition of Sn on the ANWs. The EDX pattern is shown in Fig. 3*a* and shows no traces of elements, such as C, Cr or S, indicating that the nanowires are only pure ANWs. Hence, the pure active dots around each pore were successfully worked as seeds for the growing of hexagonal arrays of ANWs on the Al substrate. The EDX pattern shown in Fig. 3*b* gives a quantitative deposition weight of 1.31% of Sn on the formed ANWs during a deposition time of 120 s.

Fig. 4 shows the XRD pattern of nanocrystallite ANWs and Sn/ANWs to confirm the structure and size of the fabricated ANWs and Sn/ANWs. The XRD pattern in Fig. 4*a* is in agreement with the cubic phase Al_2O_3 diffraction pattern (Card No. 77-0403). The diffraction peaks are observed at diffraction angles 2θ of 38.96° and 45.52°, where the intensity of the second peak is much higher than the intensity of the first peak and corresponds to the (400) plane of cubic Al_2O_3. This indicates that the crystallites have a preferential orientation towards the (400) direction. On the other hand, the XRD pattern of Sn/ANWs shown in Fig. 4*b* indicates that the major growth plane of the Sn particles is (211) at a diffraction angle of $2\theta = 44.50°$. The sharp peaks shown in this Figure are a consequence of the high crystallinity of the Sn nanoparticles. This is clearly a significance of the alignment of Sn nanoparticles on the surfaces of the straight ANWs perpendicular to the Al surface as already revealed in the SEM images in Fig. 2.

In addition, the XRD pattern in Fig. 4*b* indicates that the crystal orientation of Sn particles forms a ß-Sn tetragonal structure with a lattice constant $a = b = 5.83$ Å and $c = 3.18$ Å (Card No. 98-004-0037).

The average particle size (d) was calculated using the Scherer formula [19], $\beta = k\lambda/d \cos\theta$, where β (radians) is a full width at half maximum in the 2θ scan, k is a constant (0.94), λ is the X-ray wavelength (1.54 Å for Cu kα) and θ is the diffraction angle. Using this formula and the XRD pattern, the average size of Sn particles at $2\theta = 44.50°$ was found to be 15 nm. This size is very close to that measured by SEM. This fact simply means that the nanoparticles obtained by the above method are

Table 1 Summary of the resulting structural parameters

t_{etch}, min	D_P, nm	d_w, nm	Observations	Morphology
0	45	80	• The hexagonal order and the uniformity of the AAO templates increased as the etching time increased • A linear increase in the pore diameter as the etching time increased • Etching rate = 0.731 nm/min	nanoporous AAO membrane
30	62	63		
90	111	14		
100	118–125	7–0	Cracks appeared on the AAO wall, which was an indication of ANWs formation	2D ANWs
110	—		ANWs of length 1.23 µm and diameter 36 nm are formed	
120	—		ANWs are completely etched from the Al substrate to be free standing	1D ANWs

(Pore diameter, D_P and wall thickness, d_w) and morphologies for self-organised AAO membranes at different etching times (t_{etch})

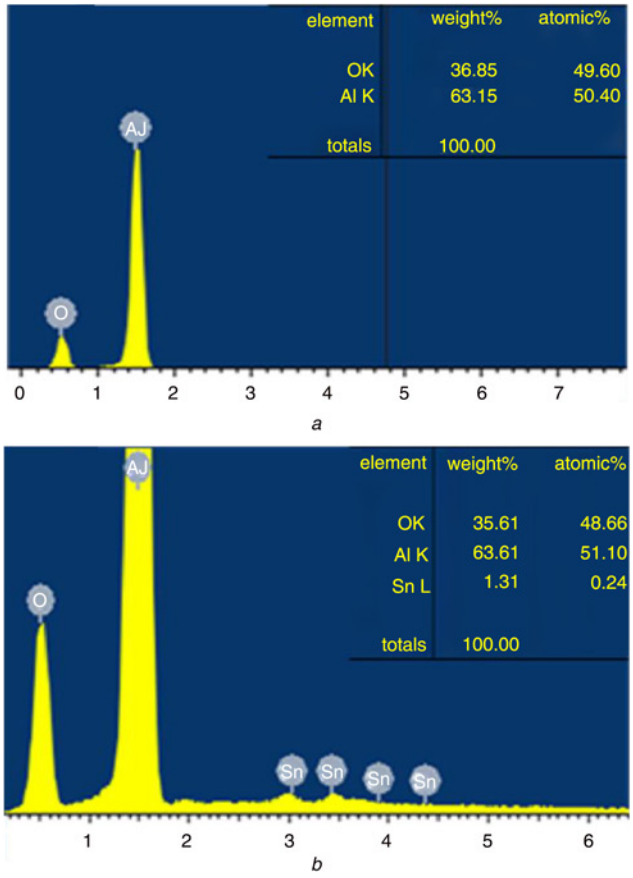

Figure 3 *EDX spectra of ANWs and Sn/ANWs*
a ANWs
b Sn/ANWs

doi: 10.1049/mnl.2015.0068

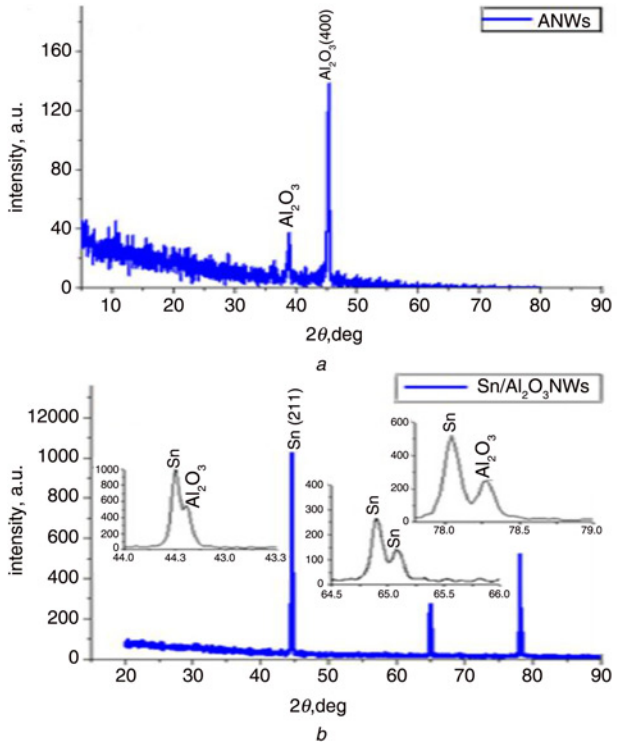

Figure 4 *XRD patterns of ANWs and Sn/ANWs*
a ANWs
b Sn/ANWs

nanocrystallites and in good agreement with the measured size of the Sn particles.

Fig. 5 comprises schematic diagrams illustrating the growth mechanism of the ANWs and the Sn/ANWs. The AAO membrane consists of hexagonal cells, each surrounding a cylindrical pore grown perpendicularly to the initial Al surface [20, 21]. The cell of AAO is composed of two different layers [22–25]: (i) an inner layer that forms the common internal walls between the AAO pores, which is relatively pure Al_2O_3; and (ii) the outer layer that surrounds the AAO pore, which consists of Al_2O_3 and negative ion impurities ($C_2O_4^{-2}$ and OH^-). These two layers form the pores walls and the barrier layer at the bottom of the pores [22]. Under the etching process, the inner layer is more resistant to be etched than the outer oxide layer with anion-incorporated Al_2O_3 [18]. The AAO consists of ordered hexagonal cells containing circular pores at the centre, and a joint area exists among three neighbouring pores (active dots), as indicated in Figs. 5*a*, *b* and 2*a*. When the phosphoric acid solution diffuses into the pores the pore walls are dissolved from the attack of H^+ or OH^- with the pore wall according to the following chemical reaction [26]

$$2OH^- + Al_2O_3 \rightarrow 2AlO^{2-} + H_2O \quad (1)$$

$$6H^+ + Al_2O_3 \rightarrow 2Al^{3+} + 3H_2O \quad (2)$$

As a consequence, the pore size is broadened and the thickness of the wall is decreased by increasing the etching time as illustrated in Figs. 5*c* and 2*b*. With increasing etching time, the interpore layer between the two adjacent pores is completely dissolved whereas the corner region (active dots) is partially dissolved because it is the thickest portion of the pure Al_2O_3 [21] as shown in Figs. 5*d* and 2*c*. The breaking areas of the cells would locate at the centres of the cell walls. In this case nanowires are formed from the remains of Al_2O_3 at the corners of the cells as indicated in Figs. 5*e*, *f* and 2*d*. When all pores expand homogeneously, under perfect conditions a nanowire could be formed in every active dot. Then, a high yield of 2×10^{10} NWs/cm^{-2} can be fabricated in this way.

The reflection spectra of the Al_2O_3 and Sn/ANWs measured at an incident angle of 5° are shown in Fig. 6. The wavelength was increased from 200 to 2000 nm in increments of 5 nm. The recorded spectra were normalised with respect to the reflection from an Al mirror. To figure out the effect of light scattering, reflection has been carried out using both specular and diffuse configurations. The obtained results should agree between the obtained patterns by the two configurations within the experimental errors. This means that the effect of roughness on the total reflectance is weak over the wavelength investigated. This may be ascribed to the very small size of the deposited Sn nanoparticles as indicated by the SEM images in Fig. 2*f*. Moreover, it is evident that the scattering has very limited effect and can be neglected. There are interesting features in the reflectance spectra of ANWs and Sn/ANWs

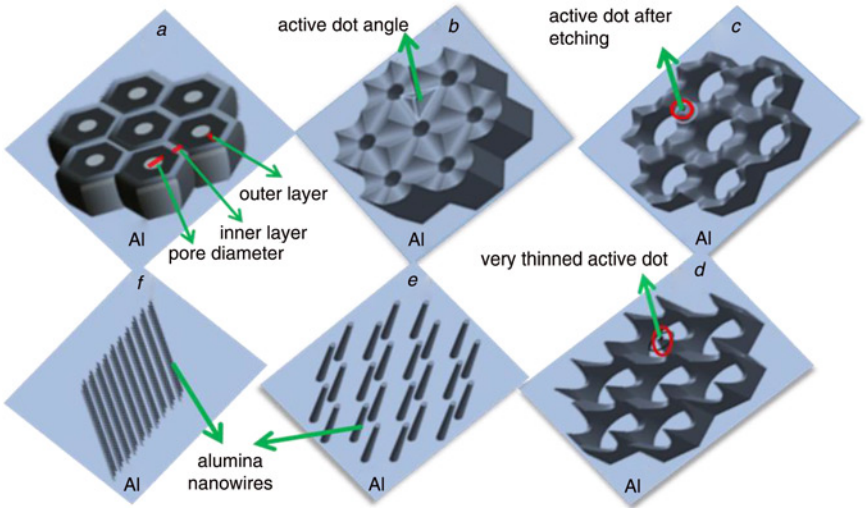

Figure 5 *Schematic diagrams illustrating the formation mechanism of the ANWs from AAO*
a Original structure of AAO with inner and outer layers
b Active dot angle
c Expanded pores with active dot after etching
d Thinned active dot of every three cells
e and *f* Final ANWs

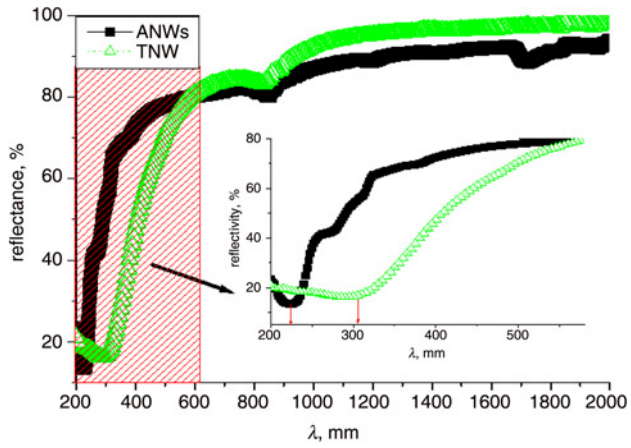

Figure 6 *Reflectance spectra of ANWs and Sn/Al_2O_3 NWs (TNWs)*

over the wavelength investigated. First, for the ANWs spectrum (black line in Fig. 6), there is an absorption band at 847 nm that can be ascribed to the existence of the AAO barrier layer and the two absorption bands at 276 and 320 nm are in coincidence with the Al_2O_3 absorption bands. Secondly, it is clear that the reflectivity of the Sn-coated ANWs slightly increased, reaching nearly 100% compared with that of blank ANWs in the NIR region, and changed smoothly with wavelength. Finally, there is an interesting redshift in the absorption band from 225 to 310 nm. To explore the reason for this redshift, a glass slide was coated with Sn under the same conditions for 90 and 120 s and the reflection spectra of these samples were measured by the same configuration.

Fig. 7*a* shows the SEM image of a glass slide coated with Sn for 120 s. This Figure shows the grown Sn nanorods with an average diameter of ~30 nm on the glass slide. Fig. 7*b* illustrates the reflection spectra of the two samples. For the sample coated for 90 s there are two modes of transverse surface plasmons (TSPs); a fundamental mode at $\lambda = 310$ nm and a higher mode at 212 nm [12, 27]. The absence of longitudinal surface plasmon (LSP) for this sample indicates that almost all Sn nanoparticles of spherical shapes have been deposited on a glass substrate. After 120 s deposition, the TSP modes are slightly blueshifted, as shown in the inset Table in Fig. 7*b*, and the weak LSP mode is centred at 700 nm. As a consequence, the shape of the nanoparticles may change from spherical to non-spherical. The departure from the spherical symmetry of the nanoparticles is ascribed to the plasmonic coupling effect between the closely distributed nanoparticles on the surface of the glass slide. Regarding Figs. 6 and 7, the redshift and broadening in the absorption band of Sn/ANWs can be ascribed to the interference between the absorption bands of Al_2O_3 and the TSP bands of the Sn nanostructures. These findings suggest that our simple method can be used to fabricate and functionalise ANWs with active nanoparticles for designing active devices such as new types of sensors.

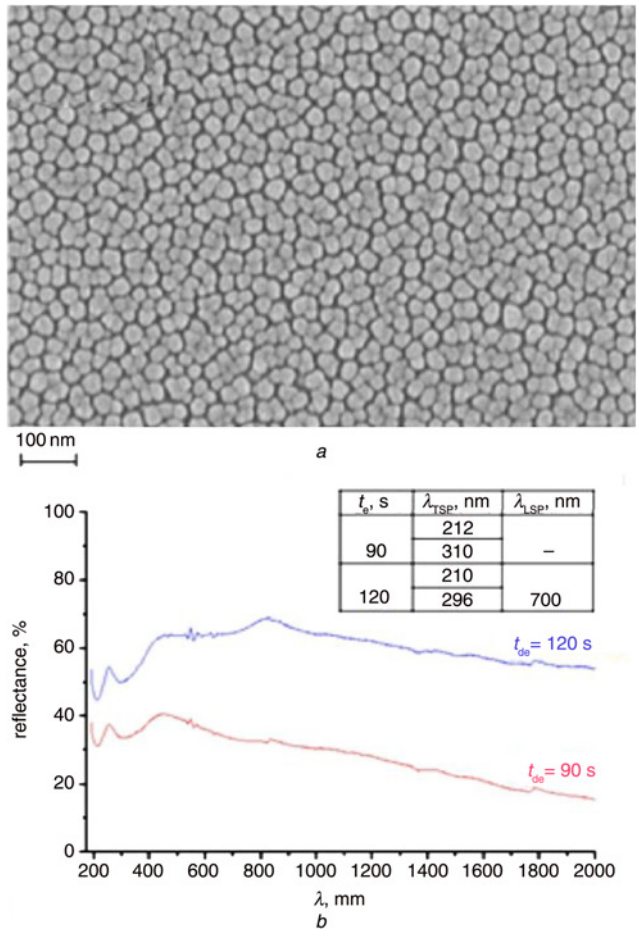

Figure 7 *SEM image of Sn on glass substrate at deposition time of 120 s, and reflection spectra of Sn/glass samples fabricated at deposition times 90 and 120 s*
a SEM image
b Reflection spectra
Variation of surface plasmon position with Sn deposition time shown in the inset Table

5. Conclusion: In this Letter, facile methods have been successfully used to fabricate ANWs and Sn/ANWs with diameters of 36 and 57 nm, respectively. The length of the fabricated nanowires can be controlled through the second anodisation time of the membrane and in this work it was controlled to a length of 1.23 μm. In addition, to obtain uniform sized ANWs the pore widening time is controlled at 110 min. The reflectance of ANWs and Sn/ANWs were measured using a UV–vis–NIR spectrophotometer and the average reflectance of Sn/Al_2O_3 slightly increased, reaching nearly 100% in the NIR region. In addition, there is a redshift and broadening in the Sn/ANWs absorption band from interference between the Al_2O_3 absorption bands and the Sn surface plasmon bands. In summary, the proposed method has merits such as low cost of processing, facile technology, a relatively simple equipment requirement and high controllability.

6 References

[1] Colinge P.J., Lee W.C., Afzalian A., *ET AL.*: 'Nanowire transistors without junctions', *Nat. Nanotechnol.*, 2010, **5**, pp. 225–229
[2] Ahn H.J., Choi J.S., Han W.J., Park J.T., Lee Y.S., Choi K.Y.: 'Double-gate nanowire field effect transistor for a biosensor', *Nano Lett.*, 2010, **10**, pp. 2934–2938
[3] Ponzoni A., Zappa D., Comini E., Sberveglieri V., Faglia G., Sberveglieri G.: 'Metal oxide nanowire gas sensors: application of conductometric and surface ionization architectures', *Chem. Eng. Trans.*, 2012, **30**, pp. 31–36
[4] Choi S.N., Yao Y., Cui Y., Cho J.: 'One dimensional Si/Sn-based nanowires and nanotubes for lithium-ion energy storage materials', *J. Mater. Chem.*, 2011, **21**, pp. 9825–9840
[5] Zhang Q., Yodyingyong S., Xi J., Myers D., Cao G.: 'Oxide nanowires for solar cell applications', *Nanoscale*, 2012, **4**, pp. 1436–1445
[6] Xia Y., Yang P., Sun Y., *ET AL.*: 'One-dimensional nanostructures: synthesis, characterization', *Adv. Mater. Appl.*, 2003, **15**, pp. 353–389
[7] Kuo G.C., Chen C.C.: 'Technique for self-assembly of tin nanoparticles on anodic aluminum oxide (AAO) membranes', *Mater. Trans.*, 2009, **50**, pp. 1102–1104
[8] Chick H., Xu J.M.: 'Nanometric superlattices: non-lithographic fabrication, materials, and prospects', *Mater. Sci. Eng. R*, 2004, **43**, pp. 103–138
[9] Kormann H.-P., Schmid G., Pelzer K., Philippot K., Chaudret B.: 'Gas phase catalysis by metal nanoparticles in nanoporous alumina membranes', *Z. Anorg. Allg. Chem.*, 2004, **630**, pp. 1913–1918

doi: 10.1049/mnl.2015.0068

[10] Schmid G.: 'Materials in nanoporous alumina', *J. Mater. Chem.*, 2002, **12**, pp. 1231–1238
[11] Yu K., Ruan G., Ben Y., Zou J.J.: 'Synthesis of carbon nanotubes within Pt nanoparticles-decorated AAO template', *Mater. Lett.*, 2007, **61**, pp. 97–100
[12] Shaban M., Hamdy H., Shahin F., Ryu S.-W.: 'Strong surface plasmon resonance of ordered gold nanorod array fabricated in porous anodic alumina template', *J. Nanosci. Nanotechnol.*, 2010, **10**, pp. 3034–3037
[13] Johansson A., Lu J., Carisson J.-O., Boman M.: 'Deposition of palladium nanoparticles on the pore walls of anodic alumina using sequential electroless deposition', *J. Appl. Phys.*, 2004, **96**, p. 5189
[14] Park W.I., Kim D.H., Jung S.W., Yi G.C.: 'Metalorganic vapor-phase epitaxial growth of vertically well-aligned ZnO nanorods', *Appl. Phys. Lett.*, 2002, **80**, pp. 4232–4234
[15] Xu C.H., Woo C.H., Shi S.Q.: 'Formation of CuO nanowires on Cu foil', *Chem. Phys. Lett.*, 2004, **399**, pp. 62–66
[16] Wang N., Cai Y., Zhang Q.R.: 'Growth of nanowires', *Mater. Sci. Eng. R*, 2008, **60**, pp. 1–51
[17] Shaban M., Hamdy H., Shahin F., Park J., Ryu S.-W.: 'Uniform and reproducible barrier layer removal of porous anodic alumina membrane', *J. Nanosci. Nanotechnol.*, 2010, **10**, pp. 3380–3384
[18] Yao L., Zheng M., Ma L., Li W., Li M., Shen W.: 'Self-assembly of diverse alumina architectures and their morphology-dependent wettability', *Mater. Res. Bull.*, 2011, **46**, pp. 1403–1408
[19] Nakade S., Matsuda M., Kambe S., *ET AL.*: 'Dependence of TiO_2 nanoparticle preparation methods and annealing temperature on the efficiency of dye-sensitized solar cells', *J. Phys. Chem. B*, 2002, **106**, p. 10004
[20] Xiao Z.L., Han C.Y., Welp U., *ET AL.*: 'Fabrication of alumina nanotubes and nanowires by etching porous alumina membranes', *Nano Lett.*, 2002, **2**, pp. 1293–1297
[21] Le Coz F., Arurault L., Datas L.: 'Chemical analysis of a single basic cell of porous anodic aluminium oxide templates', *Mater. Charact.*, 2010, **61**, pp. 283–288
[22] Choi J., Luo Y., Wehrspohn R.B., Hillebrand R., Schilling J., Gösele U.: 'Perfect two-dimensional porous alumina photonic crystals with duplex oxide layers', *J. Appl. Phys.*, 2003, **94**, pp. 4757–4762
[23] Thompson G.E., Furneaux R.C., Wood G.C., Hutchings R.J.: 'STEM/EDAX analysis of the cell walls in porous anodic films formed on aluminum', *J. Electrochem. Soc.*, 1978, **125**, pp. 1480–1482
[24] Nielsch K., Choi J., Schwirn K., Wehrspohn R.B., Gösele U.: 'Self-ordering regimes of porous alumina', *Nano Lett.*, 2002, **2**, pp. 677–680
[25] O'Sullivan J.P., Wood G.C.: 'The morphology and mechanism of formation of porous anodic films on aluminum', *Proc. R. Soc. A*, 1970, **317**, pp. 511–543
[26] Hu G., Zhang H., Di W., Zhao T.: 'Study on wet etching of AAO membrane', *Appl. Phy. Res.*, 2009, **1**, pp. 78–82
[27] Shaban M., Hamdy H., Shahin F., Ryu S.-W.: 'Optical properties of porous anodic alumina membrane uniformly decorated with ultra-thin porous gold nanoparticles arrays', *J. Nanosci. Nanotechnol.*, 2011, **11**, pp. 941–952